



Cent. Eur. J. Energ. Mater. 2025, 22(4): 511-539; DOI 10.22211/cejem/215880

Copyright © 2025 Łukasiewicz Research Network – Institute of Industrial Organic Chemistry, Poland

Article and Supplementary Information is available in PDF-format, in colour, at:

<https://ipo.lukasiewicz.gov.pl/wydawnictwa/cejem-woluminy/vol-22-nr-4/>



Article is available under the Creative Commons Attribution-Non commercial

No Derivs 3.0 license CC BY-NC-ND 3.0.

Research paper

Study on the Effect of Energetic Thermoplastic Polyurethane Elastomer on the Thermal Decomposition Performance of 5-AT/NC Energetic System

Jinyu Peng¹⁾, Bobo Zhang²⁾, Xiang Liu¹⁾, Liangyou Zhao³⁾,
Chongwei An^{1,*}, Taixin Liang¹⁾

¹⁾ School of Environment and Safety Engineering, North University of China,
Taiyuan 030051, China

²⁾ Shaanxi Qinghua Vehicle Safety Systems Co., LTD, Xi'an, 710025, China

³⁾ Luzhou North Chemical Industries Co., LTD, Luzhou, 646000, China

* E-mail: 2045786405@qq.com

Abstract: Nitrogen-rich compounds have been widely used in pyrotechnic composition and gas generators due to their high gas yield, enthalpy of formation, and environmental friendliness. However, when various nitrogen-rich compounds are used in combination with other energetic materials, adverse phenomena such as reduced thermal stability occur in the mixture. Therefore, GAP-ETPE (GAP-based energetic thermoplastic polyurethane elastomer) is selected as the coating material to enhance the thermal stability of the incompatible energetic compounds, 5-AT (5-amino-tetrazole) and NC (nitrocellulose). A relatively complete ETPE coating layer was successfully formed on the surface of 5-AT particles by solvent evaporation method. The DSC (Differential scanning calorimeter) and VST (Vacuum stability test) test results show that when 5-AT@ETPE is mixed with NC, the variation in decomposition temperature is reduced by 4.4°C, and the net increase in gas release in

the stability test is reduced by 35%. Compared with NC/5-AT, the initial activation energy of the mixed system NC/5-AT@ETPE is increased and the activation energy of the reaction process is more stable. The interaction between gas-phase products such as NO_2 with NH_2CN and HN_3 weakens, the characteristic peak of the 5-AT side reaction product NH_4 appears, and the decomposition synergy phenomenon between 5-AT and NC is weakened.

Keywords: nitrocellulose, thermal analysis, coating, 5-aminotetrazole

Supplementary Information

The decomposition peak temperatures, volumes of evolved gases and compatibility evaluation results are available in Supplementary Information.

1 Introduction

The environmental friendliness, high enthalpy of formation and gas production characteristics of nitrogen-rich compounds make them ideal materials for energetic solid fillers in propellant [1, 2]. Researchers at home and abroad have added various nitrogen-rich compounds to propellants, explosives and propellants and discovered their excellent energy properties [3-5]. However, it has been found that some nitrogen-rich compounds, such as NaN_3 , TKX-50 and other high-energy nitrogen-rich compounds, have chemical incompatibility with other energetic components [6-9]. Due to the instability of the multi-component rings of nitrogen-rich compounds [1], when mixed with other energetic materials, they show a relatively obvious effect of promoting decomposition, reducing their thermal stability and hindering their application in propellants and propellants [10].

Nitrocellulose (NC) is the most important and indispensable part of the energy component and mechanical structure framework of the propellants [11]. However, NC itself has the characteristic of chemical instability. Therefore, stabilizers such as diphenylamine are often added to the propellant to stabilize the chemical structure of NC [12]. The chemical incompatibility between nitrogen-rich compounds and NC can lead to the accelerated autocatalytic reaction of NC, accelerate the aging of the emission gas, and may affect the mechanical properties, sensitivity, storage and usage safety of the emission drug [13, 14].

Jonathan Lavoie investigated the effects of four nitrogen-rich compounds, namely 5,5'-bis(1*H*-tetrazolium)-amine (BTA), 5,5'-hydrazolium (HBT), 3,6-dizolium tetrazazine (DHT), and 5-aminotetrazolium nitrate (HAT-NO_3), on the combustion

performance of typical three-base emitants. The results show that BTA, HBT and DHT all significantly reduce the combustion temperature of the propellants, have a smaller impact on the potency of the propellant, produce more gas and have a higher proportion of N_2 . At a content of 25%, DHT and HAT- NO_3 had a significant effect on the burning rate of the propellant, which was 80% higher than that of the tribasic launching drug. The addition of nitrogen-rich compounds such as BTA, HBT and DHT all reduced the ablation effect of the propellant. The lower combustion temperature and the diffusion of nitrogen in steel and its reaction with steel effectively reduced the ablation effect of gas on the inner wall of the ablation tube. However, the addition of some nitrogen-rich compounds reduced the thermal stability of the propellant. DSC tests indicated that the addition of HBT reduced the decomposition temperature of the propellant. The analysis suggested that these two compounds might easily react with the $-ONO_2$ groups present in nitrocellulose and the plasticizers used in the formulation. Despite the presence of stabilizers, it was found that the compatibility of DHT with the nitrates used in the propellant formulation was very poor, which led to a rapid autocatalytic decomposition reaction of NC. In the vacuum stability test, the venting volume of the nitrogen-rich propellant containing HAN- NO_3 increased significantly, and the nitrogen-rich gun propellant containing DHT even experienced combustion. The compatibility of HAT- NO_3 with the same materials is also poor [15-17].

5-Aminotetrazole (5-AT) is an energetic material with a simple structure among tetrazole compounds, featuring a nitrogen content as high as 82.4% and a relatively high standard molar enthalpy of formation (208.7 kJ/mol) [18]. The synthesis technology of 5-AT is relatively mature, thus it is cheap and readily available, and has broad application prospects in gas generators, low-characteristic signal solid propellants, environmentally friendly gas, and high-energy insensitive explosives [19, 20]. However, 5-AT has significant interactions with various energetic materials such as NC, absorption tablets, NQ, RDX, and CL-20, resulting in poor compatibility with the commonly used components of emission gas and hindering its wide application in emission gas [21].

At present, there are many methods to improve the thermal stability and compatibility of materials and composites. Available stabilization strategies include inert coatings, surface passivation and doping. Surface passivation methods aim to construct a complete oxide layer on the surface through acid etching, heat treatment or other related methods to reduce external irritation [22, 23]. However, heat treatment in an air atmosphere may cause aging of energetic materials or even thermal decomposition due to the increase in temperature. The ion doping method involves adding ions to the

synthesis or crystallization of energetic materials to make the stacking structure of the molecular lattice more compact, thereby enhancing thermal stability and compatibility [24]. However, it will cause energy loss due to the introduction of doping elements. This method is mainly used to improve the thermal stability of energetic materials, but its effect on improving compatibility is relatively small.

The surface coating method is to form a coating layer of inert materials on the surface of energetic materials, thereby blocking the contact between incompatible energetic materials. It is an effective and convenient way to improve the compatibility between energetic materials. The high bond energy (451.1 kJ/mol) of the Si–O bond in silane coupling agents endows them with excellent thermal stability and they are often used to improve the thermal stability and compatibility of energetic materials. The effect of improving the compatibility of TKX-50, AlH₃ and other energetic components is relatively good [25-27]. High-efficiency coating technologies such as polydopamine (PDA) and long-chain alkanolic acid (PA) can also significantly improve the compatibility between energetic materials [28-30]. However, in the experiments to improve the chemical compatibility among energetic materials, the amount of coating used is relatively large, which has a significant impact on their energy performance. Therefore, the use of energy-containing compounds for coating can reduce energy loss. There are mainly two types of traditional energetic coating materials: One type is energetic compounds, including triaminotrinitrobenzene (TATB), 2,4,6-trinitrotoluene (TNT), and 3-nitro-1,2,4-triazole-5-one (NTO) [31, 32]. One type is energetic polymer materials, such as NC, polyazide glycidyl ether (GAP), BAMO-THF copolymer ether, energetic thermoplastic elastomer (ETPE). The selection of energetic compounds such as TATB and NTO as coating materials can reduce the energy loss of the system. However, most of the solvent systems used for coating are water, which has a relatively high solubility for 5-AT, and the energy content will also have an impact on the thermal stability of the samples [33]. GAP has a high-energy N₃ group. As a coating layer, it can achieve coating modification while reducing energy loss [34]. The isocyanate curing agent used in GAP polymerization has a strong reaction with the -NH₂ group of 5-AT, as shown in Equation 1 [35], which prevents GAP from in-situ polymerization and curing on its surface. BAMO-THF also requires the use of isocyanate curing agents for cross-linking and curing.



Energetic thermoplastic polyurethane elastomer (ETPE) is often used as an energetic binder for propellants, which can contain multiple energy groups and improve energy performance. Gap-based energetic thermoplastic polyurethane elastomer (GAP-ETPE) is a two-phase block copolymer composed of the soft segment part and the hard segment part with GAP as the prepolymer, and it has a relatively high heat of formation [36]. Therefore, ETPE can be used as an ideal energetic coating material for nitrogen-rich compounds.

In summary, to address the incompatibility between 5-AT and NC, a surface coating method was used to prepare 5-AT@ETPE coated samples, and the degree of coating was characterized by SEM and XPS. The improvement of the compatibility issue between 5-AT and NC by the coating method was investigated through differential scanning calorimetry (DSC) and vacuum stability test (VST). The improvement mechanism of coating on the mutually promoting decomposition effect was further studied through the thermal decomposition kinetics and the analysis of the pyrolysis products of the samples.

2 Experimental Section

2.1 Materials

5-AT (98%), tetrahydrofuran (99.5%) and heptane (99.5%) were purchased from Shanghai Aladdin Biochemical Technology Co., Ltd. GAP-ETPE with an average molecular weight of 31000 g/mol was supplied by the Beijing Institute of Technology. The nitrocellulose (NC, 12.7% nitrogen content) was received from Luzhou North Chemical Industry Co., Ltd.

2.2 Preparation of composites

According to the experimental conditions in Table 1, a certain amount of ETPE was dissolved in 60 mL of tetrahydrofuran, and then the corresponding amount of 5-AT was added, stir for 30 min and disperse by ultrasonic (power 100W) for 30 min. At a certain stirring rate, 30 mL of heptane is added as the continuous phase of the solution, and then the tetrahydrofuran solvent is heated and evaporated. When the solvent in the beaker has completely evaporated, add n-heptane, filter, wash the sample and dry it. Particle samples of 5-AT@ETPE were obtained.

Table 1. Coating experimental factors and experimental arrangements

Sample	ETPE [g]	5-AT [g]	Temperature [°C]	Stirring rate [r/min]
ATE1	0.125	0.875	30	875
ATE2	0.15	0.85		
ATE3	0.175	0.825		
ATE4	0.15	0.85	50	
ATE5			70	
ATE6			30	800
ATE7			30	950

2.3 Characterization of surface coatings

The surface morphological features of 5-AT and its composite 5-AT@F2602 were systematically characterized using field-emission scanning electron microscopy (FE-SEM, ZEISS Sigma 300). The proportion of surface elements of each sample was analyzed by X-ray photoelectron spectroscopy (XPS, Thermo Scientific ESCALAB 250Xi). Calculate the coverage degree by using the element content measured by XPS according to Equation 2.

$$R = \frac{N_{ATE} - N_{5AT}}{N_E - N_{5AT}} \quad (2)$$

where N_{5AT} is the proportion of N element on the 5-AT surface; N_E is the proportion of N element on the surface of ETPE. N_{ATE} is the proportion of N element on the surface of ATE samples; R is the degree of coverage.

2.4 Thermal decomposition and vacuum stability of composites

The thermal stability and component compatibility of the binary mixture were evaluated using differential scanning calorimetry (Mettler DSC3+). Samples were prepared by homogenizing NC and 5-AT samples in heptane (1:1 mass ratio) through continuous mechanical agitation for 2 h. DSC measurements were conducted under argon purge (50 mL/min) using hermetically sealed aluminum crucibles, with temperature ramping from 25 to 300 °C. The heating rate is 10 K/min.

Gas evolution behavior of the NC/5-AT composite was quantitatively analyzed using a Vacuum Stability Tester (Beijing Di'an 200Pro). Precisely weighed samples (5.000 ± 0.0001 g, 1:1 mass ratio) underwent degassing in specialized reaction vessels

evacuated to <0.5 kPa prior to isothermal conditioning at 100.0 ± 0.5 °C for 40 h. The data acquisition at 1 min intervals recorded pressure-time profiles.

2.5 Analysis of thermal decomposition characteristics

The reaction kinetics calculation was carried out based on the test sampling data of thermogravimetric analysis (TG). The improvement effect of the coating on the compatibility of NC/5-AT can be better understood by comparing the activation energy results of the thermal decomposition reaction of NC/5-AT with those of the thermal decomposition reaction process of NC/5-AT@ETPT. The TG experiment was conducted using Mettler equipment, with an atmosphere of argon (gas flow rate 50mL/min), and heating rates of 5, 10, 15, and 20 K/min. The samples were placed in sealed aluminum crucibles for testing.

In this study, the Feinn-Wall-Ozawa (FWO) [37] and Advant-Vyazovkin [38] methods were adopted to calculate the kinetic parameters of non-isothermal decomposition. The evolution process of the dynamic calculation equation is as follows.

In the heterogeneous solid thermal decomposition reaction system, using the one-step reaction kinetics equation in the isothermal homogeneous system, Arrhenius [39] can be expressed as Equation 3.

$$k(T)f(\alpha) = Af(\alpha)\exp\left(-\frac{E}{RT}\right) \quad (3)$$

where E is the activation energy of thermal decomposition reaction (J/mol); A is the reaction preexponent factor (min^{-1}); R is the gas constant (8.314J/K); T is the thermodynamic temperature (K); $f(\alpha)$ is the differential kinetic mechanism function determined by the reaction type. α is the conversion rate of the reaction, which can be calculated by Equation 4.

$$\alpha = \frac{m_0 - m_t}{m_0 - m_f} \quad (4)$$

where m_0 , m_t , and m_f represent the initial mass of the sample, the mass of the sample at time t or temperature T , and the final residual mass. And the value of α is between 0 and 1, which is a physical quantity used to represent the degree of progress of thermal decomposition reaction in heterogeneous systems.

The reaction rate equation of non-homogeneous system under non-isothermal conditions can be expressed by Equation 5.

$$\beta \frac{d\alpha}{dT} = Af(\alpha) \exp\left(-\frac{E}{RT}\right) \quad (5)$$

where β is the heating rate (K/min)

Model-free methods allow the kinetic parameters to be evaluated without pre-selecting the reaction model. In this study, Kissen-Akahira-Sunose (KAS), and Advanced-Vyazovkin methods were selected to calculate the kinetic parameters of non-isothermal decomposition. The calculated data are obtained from the relationship between mass and temperature measured by TG.

According to the KAS method, for a given value of A , the slope of the line generated by the linear correlation of $\ln(\beta/T^2)$ with $1/T$ can determine E , as shown in Equation 6.

$$\ln\left(\frac{\beta}{T^2}\right) = \ln\left(\frac{QR}{Eg(\alpha)}\right) - \frac{E}{RT} \quad (6)$$

The Advanced-Vyazovkin method has a good tolerance for experimental test fluctuations, and is a more accurate calculation method for reactions with faster decomposition rate. The method uses the activation energy as an integral expression of temperature or time function to estimate. This method is a nonlinear equivalent transformation method. For a series of TGA runs at different heating rates, the value of the $E\alpha/\alpha$ dependence can be determined by minimizing the following Equation 7.

$$\Omega(E_\alpha) = \sum_{i=1}^n \sum_{i \neq j}^n \frac{I(E_\alpha, T_{\alpha,i})\beta_j}{I(E_\alpha, T_{\alpha,j})\beta_i} \quad (7)$$

The temperature integral in the above equation can be derived from Equations 8 and 9.

$$I(E_\alpha, T_\alpha) = \int_0^{T_\alpha} \exp\left(\frac{-E_\alpha}{RT}\right) dT \quad (8)$$

$$I = \frac{E_\alpha}{R} p(x) \quad (9)$$

The temperature integral $p(x)$ in the formula is difficult to solve using numerical methods. In this paper, we solve it by using the following approximate method as Equation 10.

$$p(x) \approx \frac{\exp(-x)}{x} \times \left(\frac{x^5 + 40x^4 + 552x^3 + 3168x^2 + 7092x + 4320}{x^6 + 42x^5 + 630x^4 + 4200x^3 + 12600x^2 + 15120x + 5040} \right) \quad (10)$$

In order to study the mechanism of the interaction between NC and 5-AT in greater depth, the gas components generated during the thermal decomposition of the samples were tested and analyzed by using thermogravimetric infrared spectroscopy (TG-FTIR) analysis technology. Observe the function of the sample's mass with function of temperature or time when the sample is at a temperature controlled by the program. By combining the thermogravimetric analyzer with infrared instruments, while obtaining thermal analysis information, the escaping gases during the thermal analysis process can be further detected. The gases generated during the thermogravimetric process are sent through pipelines to the infrared spectrometer for real-time online detection. Obtain the infrared spectrum of the gas to be tested, and thereby qualitatively analyze the gas product through the relative magnitudes of the wavenumber and absorbance of the absorption peak. This can determine the composition of the product and its relationship with temperature changes, and compare it with the results of thermogravimetric analysis to gain a more comprehensive and in-depth understanding of the combustion oxidation reaction process. The test conditions adopted a heating rate of 10 K/min, an argon atmosphere flow rate of 50 mL/min, and an infrared signal acquisition frequency of 1/40 s. The tests were conducted in a synchronous analysis device (TG, Netzsch STA2500) and a spectrometer (FTIR, Thermo Fisher iS50).

3 Results and Discussion

The preparation diagram of 5-AT@ETPE is shown in Figure 1. In the mixed solution, the tetrahydrofuran solution has a relatively low solubility for 5-AT, which can wet the surface of 5-AT and cover it with the ETPE binder solution. Heat the evaporation solution to volatilize the lower boiling point tetrahydrofuran in the mixed solution

system, then ETPE precipitates from ethyl acetate and adheres to the surface of 5-AT particles to form an ETPE coating, thereby obtaining the 5-AT@ETPE sample.

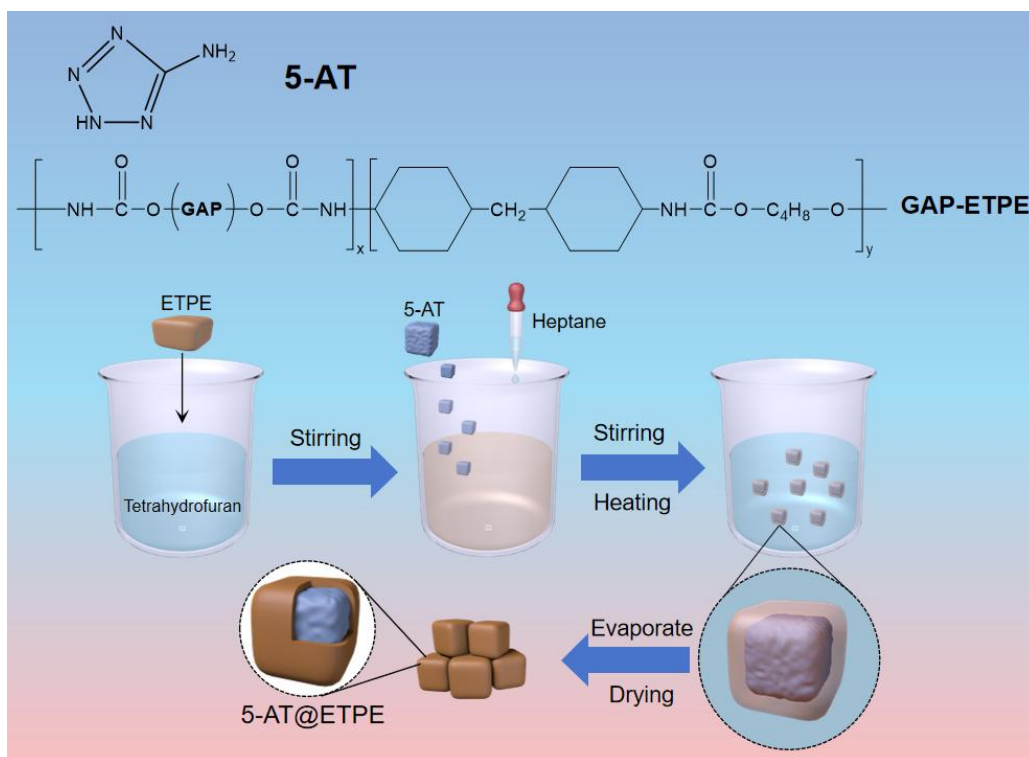


Figure 1. Schematic diagram of the preparation of 5-AT@ETPE

3.1 Morphology and structures of 5-AT@ETPE

The SEM images of 5-AT and ETPE are shown in Figure 2. 5-AT has a square structure and its surface is relatively rough. The surface of ETPE in the picture is relatively flat, presenting a continuous film-like structure with a few wrinkles, which might be caused by stress release during the solvent evaporation forming process.

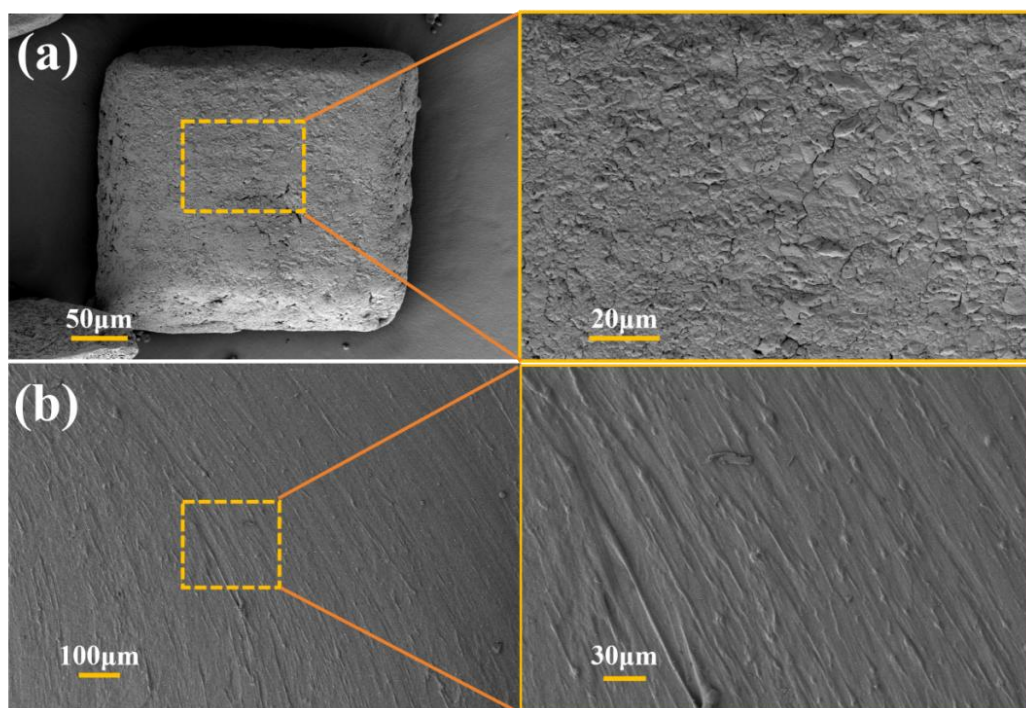


Figure 2. The SEM images of 5-AT (a) and ETPE (b)

The SEM images of the ATE samples are shown in Figure 3, where (a-g) correspond to samples 1-7 respectively. The XPS spectra of the ATE samples and their elemental contents are shown in Figure 4 and Table 1. The surfaces of samples 1, 2, 3 and 6 in the figure have a considerable number of 5-AT small particles. It might be that 5-AT has a relatively low solubility in tetrahydrofuran solution, causing the small particles to peel off from the surface. The particle structure of samples 3 and 4 of 5-AT changed into rod or needle-like agglomerated substances. The solubility of 5-AT increased in the solution at a higher temperature and it was severely etched^[33]. There are ETPE aggregates in samples 3 and 6. It might be that the amount of ETPE is excessive or the stirring rate is relatively slow, which makes ETPE prone to agglomeration during the precipitation process. The surface of sample 7 is covered with a rough continuous layer. There are no 5-AT small particles on the surface, and there are smaller ETPE aggregates beside the particles. The appropriate concentration of ETPE solution and the evaporation temperature of the solvent prevent ETPE from immediately agglomerating during precipitation and coating. Moreover, the relatively fast stirring rate enhances the dispersion of ETPE in the solution, thereby achieving a better coating effect [40]. It can be seen from Table 1 that ATE7 has the highest coverage.

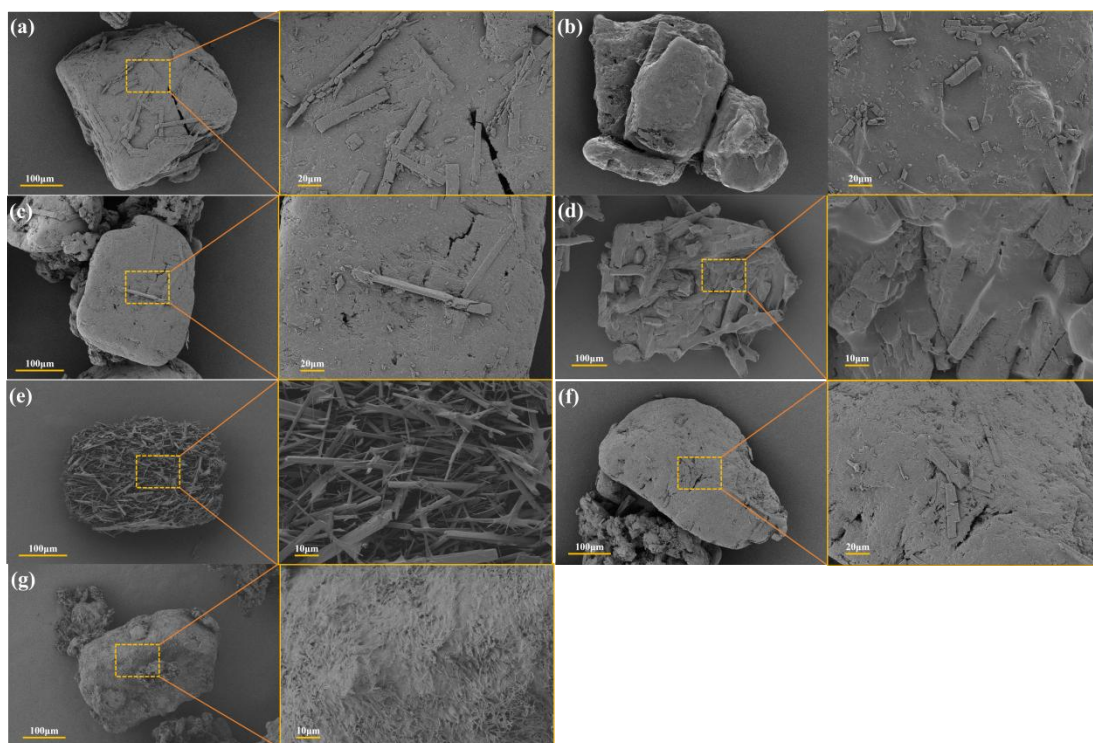


Figure 3. The SEM images of ATE samples

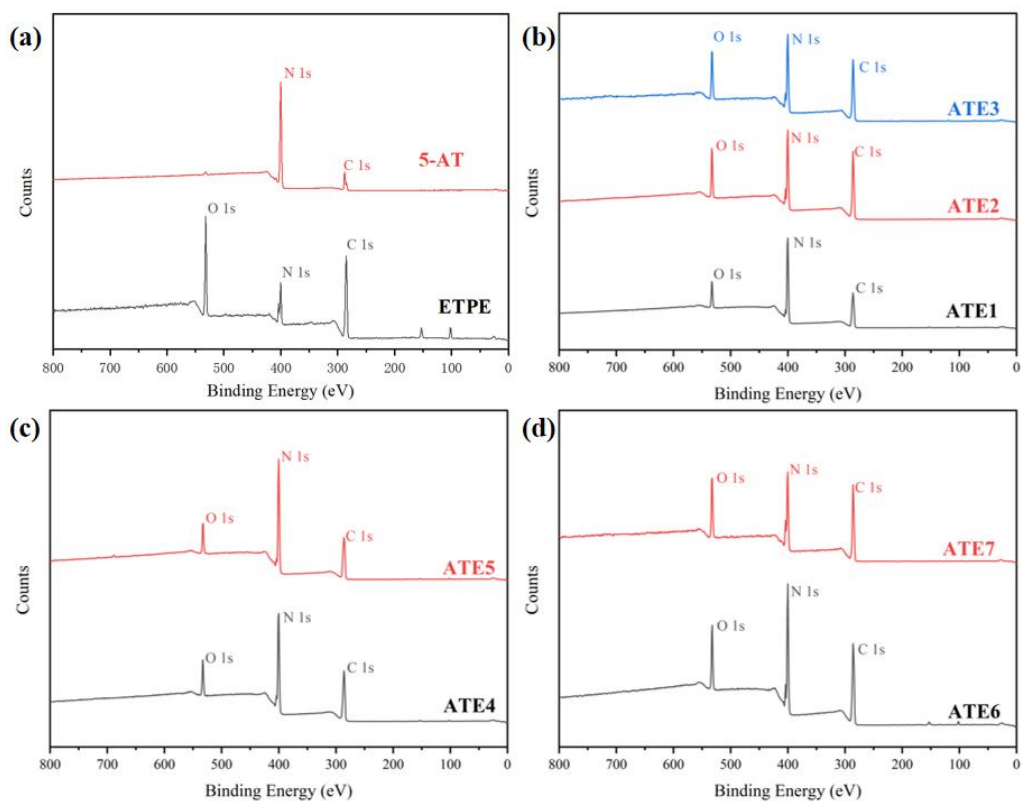


Figure 4. The XPS spectra of ATE samples

Table 2. Surface element content and coating degree of samples

Sample	Element content [%]			Coating degree [%]
	C	O	N	
5-AT	21.25	2.59	76.16	—
ETPE	53.88	26.69	19.42	—
ATE1	37.96	11.22	50.91	45.42
ATE2	49.86	17.9	32.25	76.79
ATE3	42.95	15.27	35.66	70.83
ATE4	39.85	13.73	46.42	52.01
ATE5	37.51	10.47	52.01	42.24
ATE6	44.03	14.54	41.43	60.74
ATE7	51.71	23.66	24.63	90.82

3.2 Chemical compatibility analysis

The DSC and VST experiments of all NC/ATE samples were conducted in the supplementary materials. The best-coated sample ATE7 was selected as 5-AT@ETPE to study its compatibility with NC and thermal decomposition characteristics.

3.2.1 Thermal decomposition analysis

Figure 5 shows the DSC curves of 5-AT, NC and 5-AT/NC tested under a heating rate of 10 K/min. It can be seen that 5-AT has a sharp endothermic peak at 209.2 °C. This is because 5-AT melts at this temperature and simultaneously begins to absorb heat and decompose to produce products with high enthalpy and volatility. NC has an exothermic peak at 206.8 °C. The NC/5-AT sample mixed with NC and 5-AT has only one exothermic peak, and the endothermic peak of 5-AT disappears. When NC decomposes, 5-AT is affected by the heat released by NC and melts and decomposes prematurely. The original endothermic peak of 5-AT is covered by the exothermic peak of NC, and the exothermic peak temperature of NC moves forward, forming a relatively sharp decomposition exothermic peak at 197.9 °C.

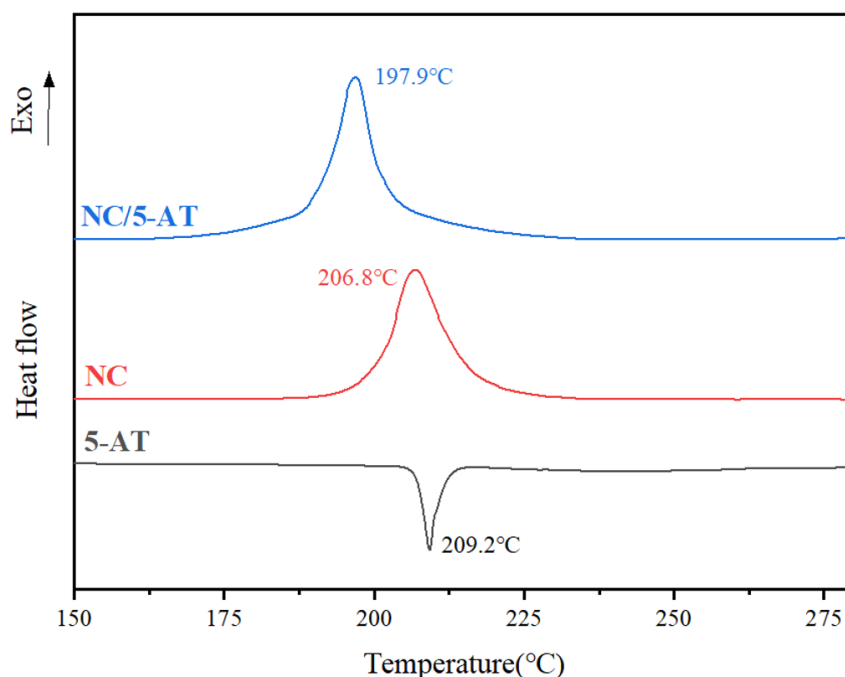


Figure 5. The DSC curve of NC and 5-AT

Figure 6(a) shows the DSC curves of ETPE, ETPE/5-AT, and ETPE/NC. In the DSC curve of ETPE, there is only one exothermic peak at 256 °C. In the ETPE/5-AT curve,

the endothermic peak of 5-AT is clearly distinguished from the exothermic peak of ETPE, and the temperatures of the exothermic peak of ETPE and the exothermic peak of 5-AT basically remain unchanged. In the curve ETPE/NC, the exothermic peaks of NC and ETPE are clearly distinguished. The temperature of the exothermic peak of ETPE is higher than that of the exothermic peak of NC, and ETPE has better thermal stability than NC. The exothermic peaks of ETPE and NC did not show significant changes in their respective peak temperatures before mixing. It is indicated that after ETPE is mixed with 5-AT and NC, the thermal stability remains good. In Figure 6(b), the peak temperature of the NC/5-AT@ETPE curve is 202.3 °C, which is 4.5 °C lower than that of the exothermic peak of NC. The exothermic peak shifted backward compared with NC/5-AT and was more gentle.

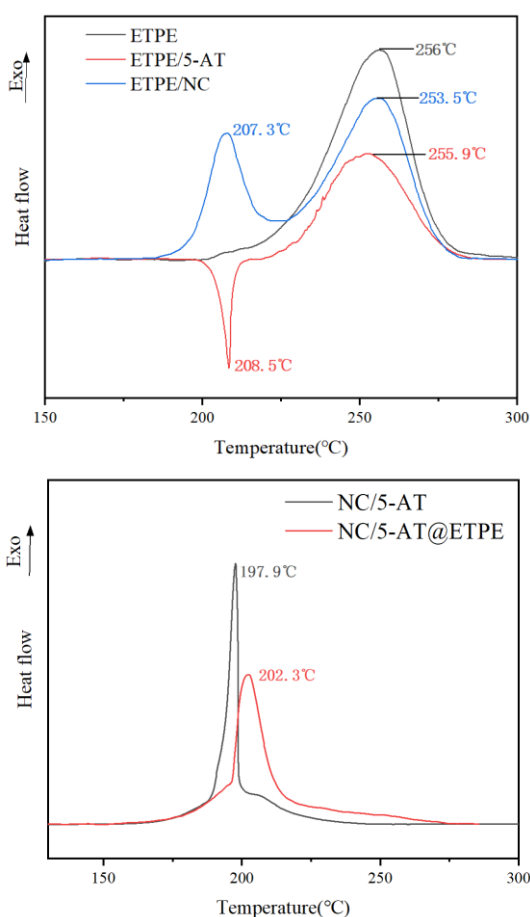


Figure 6. The DSC curve of ETPE and NC/5-AT@ETPE

3.2.2 Vacuum stability test

The DSC method measures the complete decomposition process of the system at a higher temperature, while the VST method determines the partial decomposition process at a lower temperature. The VST method is closer to the storage temperature of the system. The dynamic vacuum stability test is not only a characterization of the thermal compatibility and thermal stability of composite energetic materials, but also an important assessment of the long-term stability and safety of high-energy materials. The relationship graphs of gas release and time of NC, 5-AT and NC/5-AT in the vacuum stability experiment are shown in Figure 7. The relatively fast air release rate in the initial stage might be due to the fact that the test tube has just been placed in the heating module, and the heat inside the test tube causes the air pressure to rise. Subsequently, after the temperature of the test tube stabilized, the gas release rate of the sample stabilized.

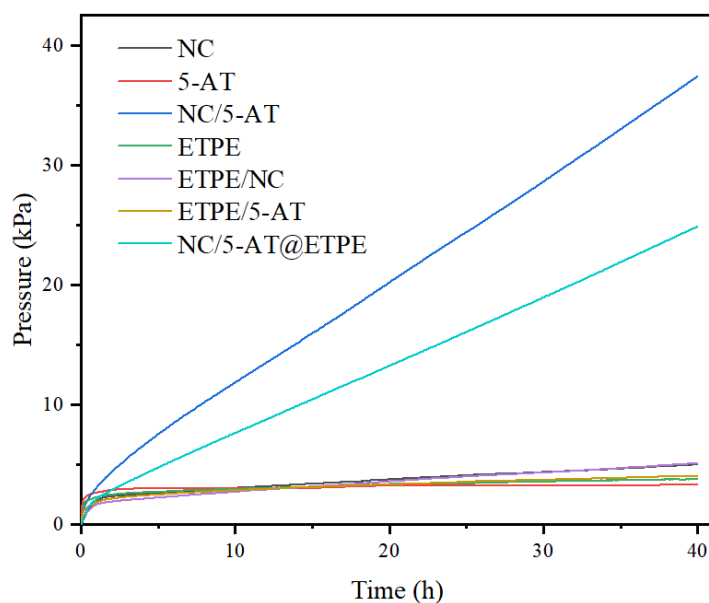


Figure 7. The evolved gases of each sample

The final amount of gas released and the net increase in gas release from the mixture reaction are shown in Table 2. The exhaust volumes of all individual samples are relatively small and all show good stability. The net reaction gas release volumes of ETPE with NC and 5-AT were 0.0446 and 0.02 mL respectively, and the compatibility evaluation grades were all compatible. It indicates that ETPE can be used as a coating material to improve the compatibility between 5-AT and NC. The gas release volume

of NC/5-AT increased significantly. The increased gas release volume due to the reaction between NC and 5-AT during the test was 7.352 mL. According to the STANAG standard, a net increase in gas release volume greater than 5.0 mL was determined to be incompatible. The discharge volume of NC/5-AT@ETPE was less than that of NC/5-AT, and the net reaction discharge volume was 4.7426 mL. After coating, the venting volume of the mixed system of 5-AT and NC decreased by 35%, indicating that the coating of ETPE effectively improved the compatibility between NC and 5-AT.

Table 2. The evolved gases and compatibility evaluation of each sample

Sample	Gas volume release [mL]	Net increase [mL]
NC	0.2732	—
5-AT	0.0204	—
ETPE	0.1065	—
ETPE/NC	0.4243	0.0446
ETPE/5-AT	0.1469	0.02
NC/5-AT	7.4817	7.3520
NC/5-AT@ETPE	5.0892	4.7426

3.3 Kinetic mechanism analysis of thermal decomposition

The TG-DTG curves of the samples under the four heating rates of 5, 10, 15, and 20 K/min are shown in Figure 8. The DTG curves of all samples shifted backward with the increase of the heating rate, which, like DSC, was the effect of the temperature gradient in the equipment.

It can be seen from Figure 8(a) that NC has only one weight loss stage in all temperature ranges, starting to decompose from around 170 °C, and the mass loss rate is about 90%. After the addition of 5-AT, NC/5-AT began to lose weight at around 160 °C, and the mass loss rate was about 75%. The decomposition temperature of NC/5-AT is about 10 °C earlier than that of NC. The peak temperature of NC/5-AT@ETPE was about 4 °C earlier than that of NC, and the weight loss rate was about 65%. A small amount of ETPE decomposes slowly at around 250 °C, and the weight loss platform is not obvious.

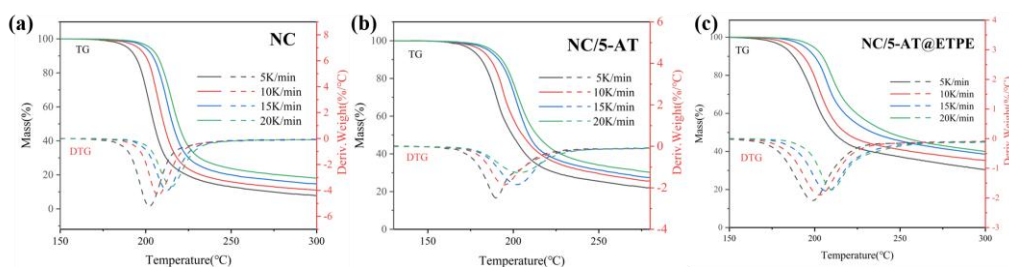


Figure 8. The TG-DTG curve of (a)NC, (b)NC/5-AT, and (c)NC/5-AT@ETPE

Figure 9 shows the conversion rates of NC, NC/5-AT and NC/5-AT@ETPE versus temperature at a heating rate of 10 K/min. After the mixture of NC and 5-AT, the decomposition temperature of NC decreased by 10-15 °C. When 5-AT@ETPE was mixed with NC, the decomposition temperature of NC decreased less than that of NC/5-AT. The reaction rate of 5-AT@ETPE with NC slows down in the early stage, and the reaction temperature is shifted back in the later stage.

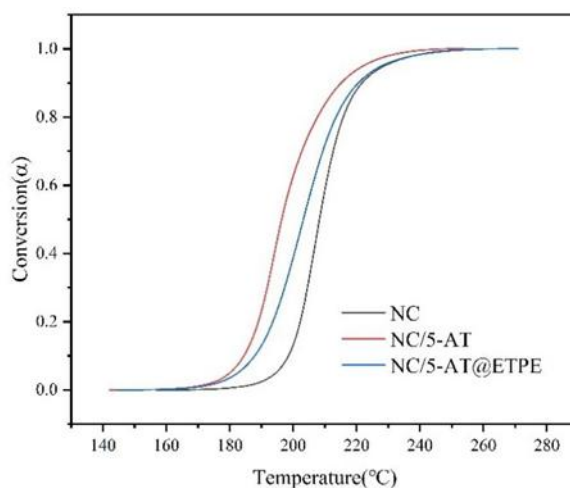


Figure 9. The curves of conversion against the temperature of NC, NC/5-AT, and NC/5-AT@ETPE

Based on the TG curves of the samples at four different heating rates measured by TG, the activation energies of NC, NC/5-AT and NC/5-AT@ETPE were calculated using FWO and Advanced Vyazovkin methods. The fitting process curves are shown in Figure 10, and the calculated activation energies are shown in Figure 11. The activation energy calculated by the two methods has the same changing trend as the

conversion rate, and the calculated activation energy is very close, confirming the reliability of the activation energy calculation.

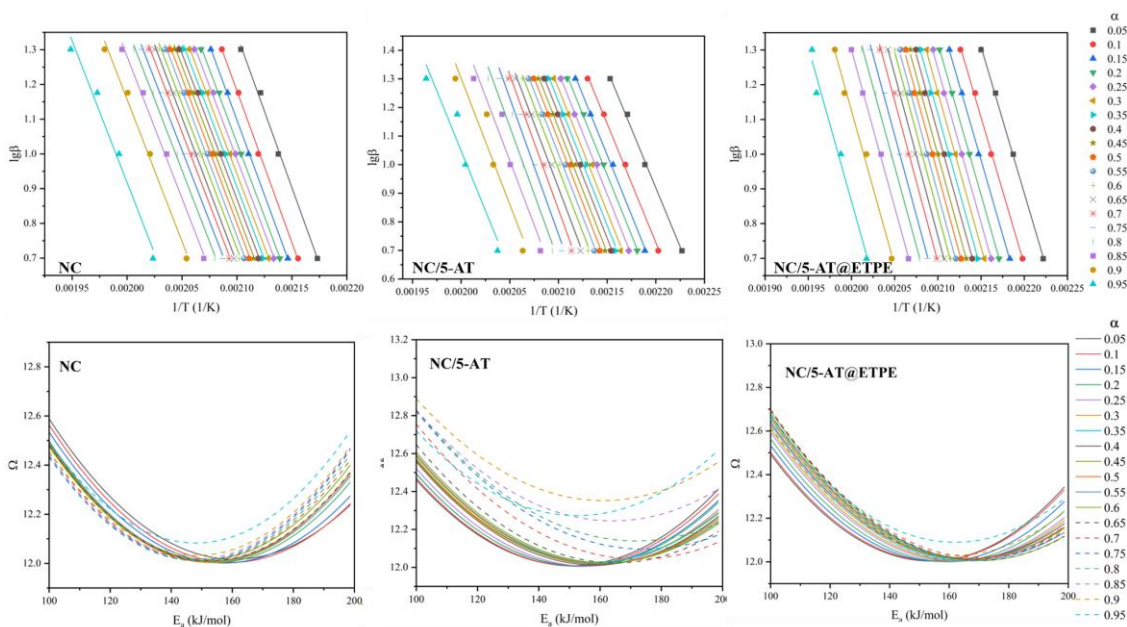


Figure 10. The fitting graphs of NC, NC/5-AT, and NC/5-AT@ETPE by FWO method (a) and Advanced-Vyazovkin method (b)

The initial activation energy of NC is 160 kJ/mol, and the activation energy decreases to 148 kJ/mol as the conversion rate increases. This is due to the autocatalytic decomposition of NC during the thermal decomposition process [12]. In NC/5-AT, the initial decomposition activation energy is 150 kJ/mol. In $\alpha \leq 0.2$, the activation energy of NC/5-AT is less than that of NC. When $0.2 \leq \alpha \leq 0.7$, the activation energy increases slowly. After $\alpha \geq 0.7$, the activation energy increased rapidly to 174 kJ/mol and then decreased to 152 kJ/mol. The decomposition temperature of ETPE in NC/5-AT@ETPE is relatively high and the content is low, which has little influence on the thermal analysis of the NC decomposition temperature range. The initial activation energy of NC/5-AT@ETPE is 153 kJ/mol. With the increase of conversion rate, the thermal decomposition activation energy of NC/5-AT@ETPE rises to 169 kJ/mol. Compared with NC/5-AT, the initial activation energy increases and the sudden increase in activation energy in the later stage is relieved.

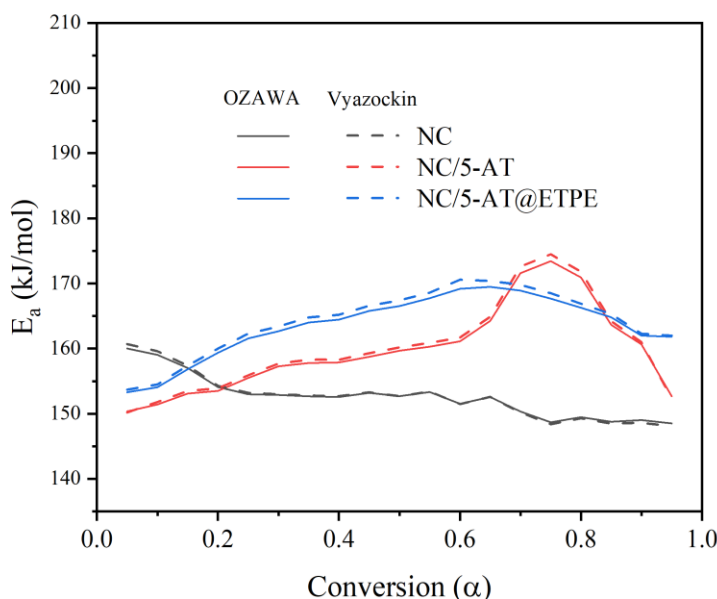


Figure 11. The Activation energy curves of NC, NC/5-AT, and NC/5-AT@ETPE

3.4 TG-IR analysis of composites

TG curves and three-dimensional infrared spectra of 5-AT, NC/5-AT and NC/5-AT@ETPE are shown in the figure. The characteristic absorption peak of 5-AT weight loss at 200~300 °C and the appearance of a large amount of gaseous products. The curves of NC/5-AT and NC/5-AT@ETPE in Figure 13 are steeper than those in Figure 8 because the reaction of the sample in an open alumina crucible is faster and more thorough than that in the TG test in a sealed aluminum crucible, but the overly rapid reaction rate is not conducive to accurate calculation of the thermal decomposition kinetics. The TG curve of NC/5-AT lost 97% at 185 °C. Before weightlessness, there is a phenomenon of weight gain. This is because the NC/5-AT sample decomposes rapidly in the open alumina crucible, and the large amount of gas generated rapidly has an instantaneous downward pushing effect on the weighing platform of TG, causing the weight to suddenly drop and then rebound. The decomposition temperature of NC/5-AT@ETPE is higher than NC/5-AT, and it loses 80% at 196 °C, with sudden weight gain disappearing before weight loss. It is indicated that the coating effect of ETPE slows down the mutually promoting decomposition effect between 5-AT and NC, and slows down the reaction rate. The weight loss at 280 °C is the decomposition of ETPE. ETPE decomposes only after the

thermal decomposition of NC is completed, indicating that ETPE still has relatively high thermal stability between 5-AT and NC.

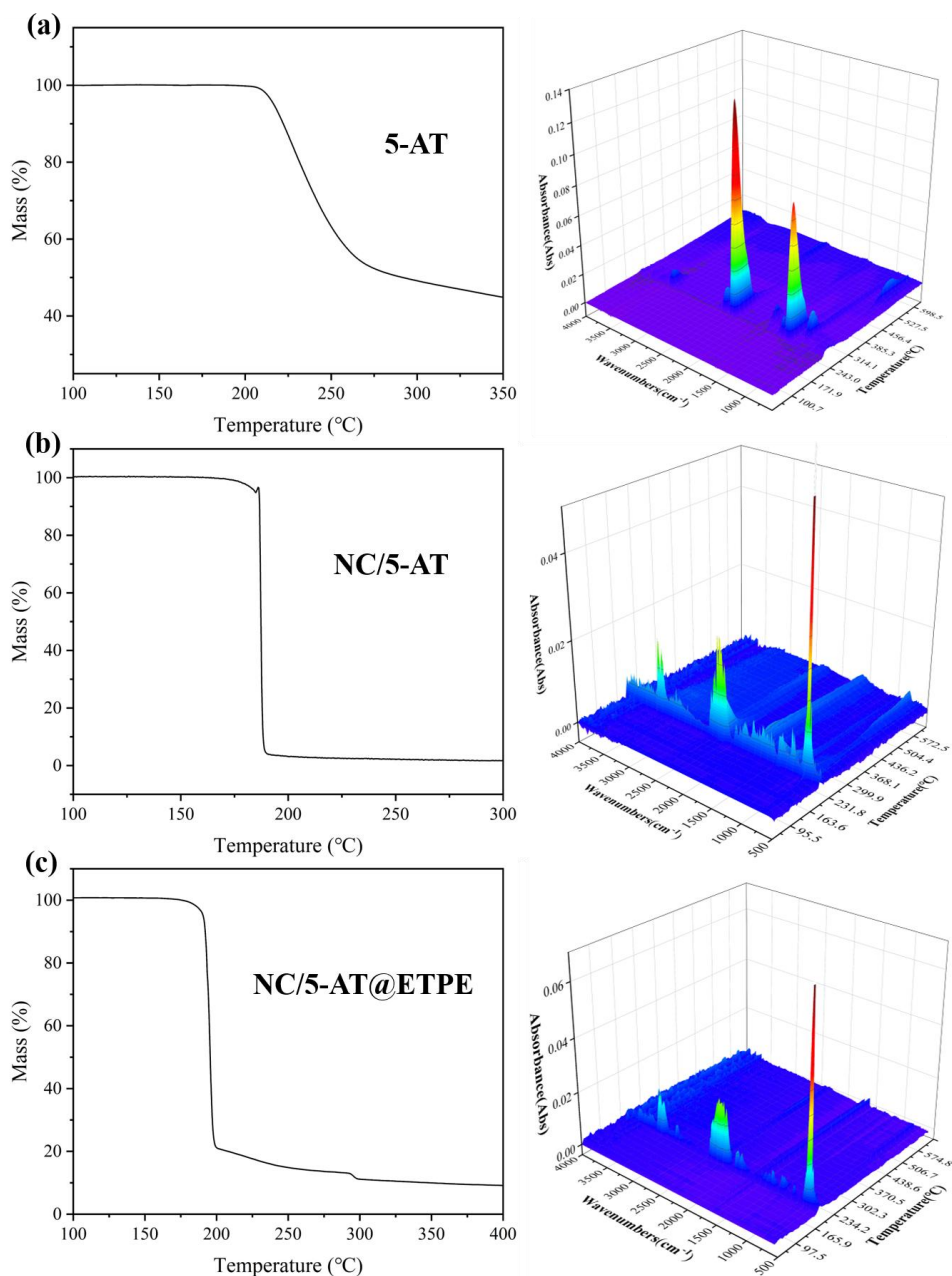


Figure 12. The TG curve and 3D-IR spectra of (a)5-AT, (b)NC/5-AT, and (c)NC/5-AT@ETPE

The IR two-dimensional diagrams of 5-AT and NC/5-AT are shown in Figure 13. In Figure 13(a) the characteristic absorption peaks at 2200-2000 and 1210-1060 cm^{-1} are the stretching vibration peaks of $\text{N}=\text{N}=\text{N}$, corresponding to the HN_3 group. 2340-2050 cm^{-1} is the stretching vibration of CN , and 3400-3200 cm^{-1} is the stretching vibration of $\text{N}-\text{H}$ in $-\text{NH}_2$, corresponding to NH_2CN . The sum of the enthalpy of formation of HN_3 and NH_2CN is greater than the enthalpy of formation of 5-AT. In the DSC curve shown in Figure 5, both the melting peak and the decomposition peak here jointly present as an endothermic peak. After 243 $^{\circ}\text{C}$, 1650-1550 cm^{-1} corresponds to the stretching vibration of $-\text{N}-\text{H}$ in NH_4^+ , and 900-990 cm^{-1} corresponds to the stretching vibration of $\text{N}-\text{H}$ in NH_3 . The products of 5-AT, NH_2CN and $\text{HN}=\text{C}=\text{NH}$, will undergo addition reactions to generate intermediate products such as melamine, which then decompose to form NH_3 , NH_4N_3 , and N_2 . N_2 has not been discovered due to its structural symmetry. After mixing with NC in Figure 13(b), the temperature at which the characteristic absorption peaks of the HN_3 group appear decreases, and the characteristic absorption peaks corresponding to NH_4^+ and NH_3 disappear. As the temperature rises, the signal characteristic peaks corresponding to CO_2 and HN_3 , $-\text{CN}$ gradually weaken and then disappear simultaneously. This is consistent with the results of other studies [41, 42].

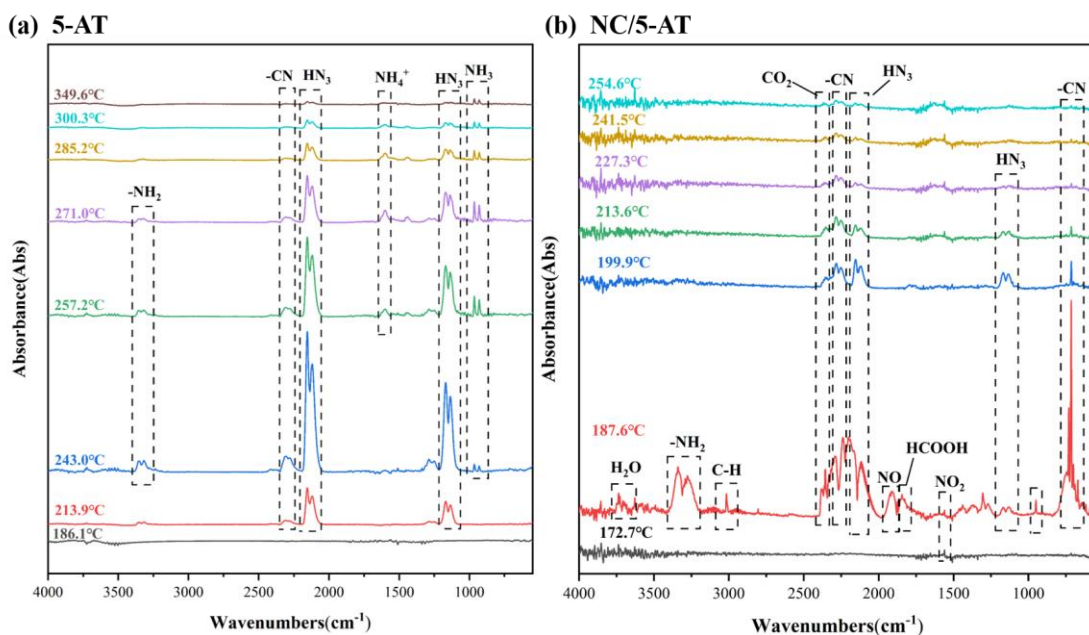


Figure 13. The 2D-IR spectra of (a)5-AT and (b)NC/5-AT

Combined with the variation trend of activation energy in Figure 11, it can be known that the initial activation energy of NC/5-AT is lower than that of NC because the heat released by the initial decomposition of NC and NO_2 catalyze the decomposition of 5-AT. In the VST test in Figure 6, the increase in the net reaction gas release volume of NC/5-AT May be due to the gas products released by the cleavage of the tetrazole ring of 5-AT. The sudden increase in activation energy at the conversion rate α of about 0.8 is due to the consumption of NO_2 initially decomposed by NC, the lack of catalysis of NO_3^- for the thermal decomposition of the remaining solid compounds, and the superposition phenomenon of multiple reactions in the mixed system [21], which leads to the increase in activation energy. NC and 5-AT show a decomposition and synergy phenomenon.

The two-dimensional infrared spectrum of NC/5-AT@ETPE is shown in the Figure 14. At 197.7 °C, the signal characteristic peaks of a large number of gas products appeared. Among them, the signal characteristic peak of $-\text{CN}$ was slightly weaker in intensity compared with the $-\text{CN}$ signal in the NC/5-AT product. With the increase of temperature, the signal strength of HN_3 in NC/5-AT@ETPE increased compared with that in NC/5-AT, and characteristic peaks of NH_4^+ and NH_3 appeared.

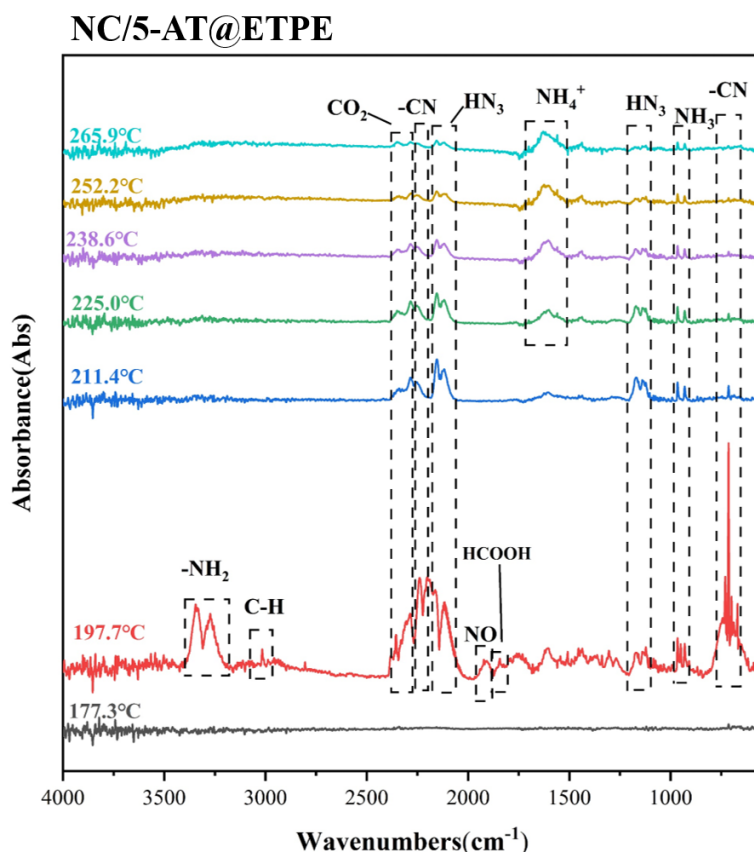


Figure 14. The 2D-IR spectra of NC/5-AT@ETPE

Combined with the activation energy shown in the Figure 11, the initial activation energy of NC/5-AT@ETPE increases and the phenomenon of sudden activation energy increase decreases. It is indicated that the coating layer of ETPE on the surface of 5-AT weakens the interaction between 5-AT and NC to a certain extent.

4 Conclusions

- ◆ A relatively complete ETPE coating layer was successfully formed on the 5-AT surface. The results of DSC and VST tests indicated that the temperature difference after mixing with NC decreased from 8.9 to 4.5 °C, and the net increase in the reaction gas release volume decreased from 7.32 to 4.74 mL. It is indicated that the ETPE coating layer effectively weakens the mutually promoting decomposition effect between NC and 5-AT. ETPE as a separation layer between 5-AT and NC, reduces the difference in the initial decomposition activation energy

between the NC/5-AT mixture and NC. The phenomenon of a sudden increase in the activation energy of NC/5-AT weakens, and the overall activation energy increases. The characteristic products (NH_4^+ and NH_3) of 5-AT appeared. 5-AT carried out the original thermal decomposition process.

- ◆ Solving the incompatibility problem between nitrogen-rich compounds and other energetic materials can greatly enhance the safety of composite energetic materials and broaden the practicality of nitrogen-rich compounds. In the future, by adopting more advanced coating technologies, efficient coating of ETPE can be achieved.

References

- [1] Damse, R.S.; Naik, N.H.; Ghosh, M.; Sikder, A.K. Thermoanalytical Screening of Nitrogen-Rich Compounds for Ballistic Requirements of Gun Propellant. *J. Propul. Power* **2009**, *25*(1): 249-256; <https://doi.org/10.2514/1.35789>.
- [2] Chen, B.; Lu, H.; Chen, J.; Chen, Z.X.; Yin, S.F.; Peng, L.F.; Qiu, R.H. Recent Progress on Nitrogen-Rich Energetic Materials Based on Tetrazole Skeleton. *Top. Curr. Chem.* **2023**, *381*(5) paper 25; <https://doi.org/10.1007/s41061-023-00435-8>.
- [3] Forquet, V.; Sabaté, C.M.; Chermette, H.; Jacob, G.; Labarthe, É.; Delalu, H.; Darwich, C. Energetic Properties of Rocket Propellants Evaluated through the Computational Determination of Heats of Formation of Nitrogen-Rich Compounds. *Chem. – Asian J.* **2016**, *11*(5): 730-744; <https://doi.org/10.1002/asia.201501204>.
- [4] Damse, R.S.; Sikder, A.K. Suitability of Nitrogen Rich Compounds for Gun Propellant Formulations. *J. Hazard. Mater.* **2009**, *166*(2-3): 967-971; <https://doi.org/10.1016/j.jhazmat.2008.12.008>.
- [5] Cao, C.; Zhang, D.; Lu, S.; Liu, C.C. Thermal Decomposition Behavior, Kinetics, Thermal Safety and Burning Characteristics of Guanidinium-5-aminotetrazole (GA) Based Propellants. *J. Therm. Anal. Calorim.* **2021**, *143*(1): 609-618; <https://doi.org/10.1007/s10973-019-09063-1>.
- [6] Huang, J.; Peng, R.; Jin, B. Premature Thermal Decomposition Behavior of 3,4-Dinitrofurazanfuroxan with Certain Types of Nitrogen-rich Compounds. *Def. Technol.* **2023**, *26*: 102-110; <https://doi.org/10.1016/j.dt.2022.07.002>.
- [7] Yao, Y.; Zhou, X.; Lin, Q.; Lu, M. Compatibility Study of NaN_3 with Traditional Energetic Materials and HTPB Propellant Components. *J. Energ. Mater.* **2020**, *38*(4): 445-454; <https://doi.org/10.1080/07370652.2020.1731016>.
- [8] Zhao, C.; Chi, Y.; Yu, Q.; Wang, X.F.; Fan, G.J.; Yu, K. Comprehensive Study of

- the Interaction and Mechanism between Bistetrazole Ionic Salt and Ammonium Nitrate Explosive in Thermal Decomposition. *J. Phys. Chem. C* **2019**, *123*(45): 27286-27294; <https://doi.org/10.1021/acs.jpcc.9b05728>.
- [9] Huang, H.; Shi, Y.; Yang, J.; Li, B.P. Compatibility Study of Dihydroxylammonium 5,5'-Bistetrazole-1,1'-diolate (TKX-50) with Some Energetic Materials and Inert Materials. *J. Energ. Mater.* **2015**, *33*(1): 66-72; <https://doi.org/10.1080/07370652.2014.889781>.
- [10] Yan, Q.L.; Li, X.J.; Zhang, L.Y.; Li, J.Z.; Li, H.L.; Liu, Z.R. Compatibility Study of trans-1,4,5,8-Tetranitro-1,4,5,8-tetraazadecalin (TNAD) with Some Energetic Components and Inert Materials. *J. Hazard. Mater.* **2008**, *160*(2-3): 529-534; <https://doi.org/10.1016/j.jhazmat.2008.03.027>.
- [11] Fu, Y.; Liu, Z.; Xu, B.; Zhu, Y.; Wang, X.J.; Yang, J.; Chen, Q.; Ma, Y.M.; Chen, F.Y.; Liao, X. Influence of Different Energetic Plasticizers on the Performance of NC-RDX Nitramine Gun Propellants. *J. Sci.:Adv. Mater. Devices* **2024**, *9*(1) paper100650.
- [12] Zhao, Y.; Jin, B.; Zheng, T.; Peng, R.F. Anti-autocatalysis Activity of Tea Polyphenols in Nitrocellulose Thermal Decomposition. *Cellulose* **2022**, *29*(17): 9089-9104; <https://doi.org/10.1007/s10570-022-04819-9>.
- [13] Trache, D.; Tarchoun, A.F.; Chelouche, S.; Khimeche, K. New Insights on the Compatibility of Nitrocellulose with Aniline-based Compounds. *Propellants Explos. Pyrotech.* **2019**, *44*(8): 970-979; <https://doi.org/10.1002/prop.201800269>.
- [14] Qi, X.; Chen, S.; Liu, X.; Yan, N.; Jin, B.; Liu, P.J.; Yan, Q.L. Comparative Study on Compatibility of Graphene-based Catalysts with Energetic Ingredients by Using DSC and VST Methods. *J. Therm. Anal. Calorim.* **2021**, *144*(4): 1139-1149; <https://doi.org/10.1007/s10973-020-09646-3>.
- [15] Lavoie, J.; Petre, C.F.; Dubois, C. Erosivity and Performance of Nitrogen-Rich Propellants. *Propellants Explos. Pyrotech.* **2018**, *43*(9): 879-892; <https://doi.org/10.1002/prop.201700272>.
- [16] Lavoie, J.; Petre, C.F.; Durand, S.; Dubois, C. Stability and Performance of Gun Propellants Incorporating 3,6-Dihydrazino-s-tetrazine and 5-Aminotetrazolium Nitrate. *J. Hazard. Mater.* **2019**, *363*: 457-463; <https://doi.org/10.1016/j.jhazmat.2018.09.088>.
- [17] Lavoie, J.; Petre, C.F.; Paradis, P.Y.; Dubois, C. Burning Rates and Thermal Behavior of Bistetrazole Containing Gun Propellants. *Propellants Explos. Pyrotech.* **2017**, *42*(2): 149-157; <https://doi.org/10.1002/prop.201600091>.
- [18] Chermahini, A.N.; Farrokhpour, H.; Eghbalsaeid, M.; Teimouri, A. DFT and MP2 Study of Intermolecular Interaction of 5-Aminotetrazole and Hydrazine:

- Enthalpy of Formation of Hydrazinium 5-Aminotetrazolate in the Gas Phase. *Propellants Explos. Pyrotech.* **2014**, 39(4): 496-503; <https://doi.org/10.1002/prep.201300182>.
- [19] He, N.; Shen, R.; DeLuca, L.T.; Wu, L.Z.; Zhang, W.; Ye, Y.H. Burning Rate Analysis of Laser Controlled 5-Aminotetrazole Propellant. *Def. Technol.* **2023**, 22: 10-27; <https://doi.org/10.1016/j.dt.2021.11.015>.
- [20] Liang, T.X.; Xiao, F.; Li, C.Z.; Seilkhan, A.; Aimbetova, E.; Aimbetova, I. Improvement of Energy Density and Thermodynamic Properties of Aluminum Powder by Assembling 5-Aminotetrazole with High Enthalpy on the Surface Layer of Aluminum Powder. *Adv. Compos. Hybrid Mater.* **2025**, 8(1); <https://doi.org/10.1007/s42114-024-01161-5>.
- [21] Zheng, D.; Wang, J.; Duo, Y.; Fangm Z.Q.; Yu, C.; Qiaom M.Z.; Liu, J.P. Experimental Insight into Co-Pyrolysis Mechanism of 5-Amino 1H-tetrazole/Nitrocellulose Based Pyrotechnic. *J. Anal. Appl. Pyrolysis* **2022**, 167 paper 105669; <https://doi.org/10.1016/j.jaap.2022.105669>.
- [22] Kato, S.; Biemann, M.; Ikeda, K.; Orimo, S.; Borgschulte, A.; Züttel, A. Surface Changes on AlH_3 during the Hydrogen Desorption. *Appl. Phys. Lett.* **2010**, 96(5) paper 051912; <https://doi.org/10.1063/1.3269598>.
- [23] Nakagawa, Y.; Isobem S.; Wang, Y.M.; Hashimoto, N.; Ohnuki, S.; Zeng, L.; Liu, S.S.; Ichikawa, T.; Kojima, Y. Dehydrogenation Process of AlH_3 Observed by TEM. *J. Alloys Compd.* **2013**, 580: S163-S166; <https://doi.org/10.1016/j.jallcom.2013.02.090>.
- [24] Matzek, N.; Roehrs, H. *Stabilization of Light Metal Hydride*. US Patent 3803082, **1974**.
- [25] Ma, L.; Xu, B.; Liao, X. Preparation of TKX-50/KH550 Composites and their Compatibility with Nitrocellulose. (in Chinese) *Chin. J. Energ. Mater.* **2022**, 1197-1204.
- [26] Shi, Z.; Tan, Q.; Wang, X.; Lu, T.; Zhang, J.; Du, Z.; Xia, D.; Lin, K.; Yang, Y. Silane Coupling Agent Modified $\alpha\text{-AlH}_3$ Materials Preparation and their Compatibility with HMX and CL-20. (in Chinese) *Chin. J. Energ. Mater.* **2023**, 662-671.
- [27] Klapotke, T.M. *Chemistry of High-Energy Materials*. 3rd Ed., deGruyter; Berlin/Boston, **2015**, p. 419; ISBN: 978-3-11-043933-5.
- [28] Qin, M.; Yao, B.; Shi, Q.; Tangm W.; Chen, S.L.; Guo, T.; Wang, W.; Zhang, Y.; Ge, Z.X. PDA Modification and Properties of $\alpha\text{-AlH}_3$. *Sci. Rep.* **2022**, 12(1):1-8; <https://doi.org/10.1038/s41598-022-16424-8>.
- [29] An, Q.; Xie, W.; Lim Y.; Jian, X.; He, X.; Wang, L.; Zhang, X.; Han, P.Y.

- Microstructure and Interaction in Aluminum Hydrides@Polydopamine Composites and Interfacial Improvement with GAP Adhesive. *Sci. Rep.* **2024**, *14*(1) paper 10013; <https://doi.org/10.1038/s41598-024-59944-1>.
- [30] Li, J.; Du, F.; Tang, C.; Yang, Y.; Xia, D.; Zhang, J.; Wang, P.; Lin, K. Stabilization Coating of Aluminum-Lithium Alloy and Its Application in Propellant. (in Chinese) *Chin. J. Energ. Mater.* **2024**, *32*(1): 2-11.
- [31] Zhang, S.; Zhan, L.W.; Teng, Y.Y.; Yang, X.B.; Xiao, L.; Hao, G.Z.; Hou, J.; Li, B.D. Layer-by-Layer Nano-TATB Coating for HMX Surface: A Scalable Method to Achieve the High-Energy and Low-Sensitivity Explosive. *Sci. Technol. Energ. Mater.* **2021**, *82*(6): 152-160.
- [32] Lan, G.C.; Gu, G.H.; Wang, Y.C.; Zhang, G.Y.; Wang, J.L.; Li, J. Preparation of HMX@DHBA-Pb and HMX@NTO-Pb Composites via In Situ Deposition: A Way to Achieve Surface Catalysis of HMX. *Arabian J. Chem.* **2023**, *16*(8) paper 104915; <https://doi.org/10.1016/j.arabjc.2023.104915>.
- [33] He, Z.; Zhang, J.; Gao, X.; Tang, T.; Yin, X.F.; Zhao, J.; Li, R.R.; Han, D.M. Solubility Determination, Correlation, and Solute-Solvent Molecular Interactions of 5-Aminotetrazole in Various Pure Solvents. *J. Chem. Eng. Data* **2019**, *64*(9): 3988-3993; <https://doi.org/10.1021/acs.jced.9b00385>.
- [34] Zeng, C.; Yang, Z.; Wen, Y.; He, W.; Gong, F. Performance Optimization of Core-Shell HMX@(Al@GAP) Aluminized Explosives. *Chem. Eng. J.* **2020**, *407*(2) paper 126360; <https://doi.org/10.1016/j.cej.2020.126360>.
- [35] Liu, L.; Yu, S.; Zhou, Y.; Gao, C. Study on a Novel Polyamide-Urea Reverse Osmosis Composite Membrane (ICIC-MPD): I. Preparation and Characterization of ICIC-MPD Membrane. *J. Membr. Sci.* **2006**, *281*(1-2): 88-94; <https://doi.org/10.1016/j.memsci.2006.03.012>.
- [36] Zhang, X.M.; Wu, W.; Jin, P.; Ding, S.J.; Liu, S.; Zhao, S.; Yang, W.; Liu, W.H.; Luo, Y.J. Effect of Azide Polyether Pyrolysis Property on Combustion and Heat Release of Boron-based Fuel-rich Propellant. *Combust. Flame* **2022**, *245* paper 112269; <https://doi.org/10.1016/j.combustflame.2022.112269>.
- [37] Sun, Y.; Ren, H.; Jiao, Q. Comparison of Thermal Behaviors and Decomposition Kinetics of NEPE Propellant Before and After Storage. *J. Therm. Anal. Calorim.* **2018**, *131*(1): 101-111; <https://doi.org/10.1007/s10973-017-6525-8>.
- [38] Vyazovkin, S.; Sbirrazzuoli, N. Isoconversional Kinetic Analysis of Thermally Stimulated Processes in Polymers. *Macromol. Rapid Commun.* **2006**, *27*(18): 1515-1532; <https://doi.org/10.1002/marc.200600404>.
- [39] Crapse, J.; Pappireddi, N.; Gupta, M.; Shvartsman, S.Y.; Wieschaus, E.; Wühr, M. Evaluating the Arrhenius Equation for Developmental Processes. *Mol. Syst.*

- Biol.* **2021**, *17*(8) paper MSB20209895; <https://doi.org/10.15252/msb.20209895>.
- [40] Lim, M.; Jang, Y.; Kim, H.; Rhee, H.; Noh, S. Synthesis and Characterization of Alkoxy and Alkylamino GAP Copolymer for Energetic Thermoplastic Elastomer (ETPE). *Appl. Chem. Eng.* **2019**, *30*(1): 81-87; <https://doi.org/10.14478/ace.2018.1116>.
- [41] Li, C.; Jia, H.; Li, W.; Ding, Y.J.; Xiao, Z.L.; Zhou, J.; Li, S.Y. Investigation of the Reaction Mechanism of 5-Amino-1H-Tetrazole with Nitrocellulose Using Thermal Analysis Techniques. *J. Anal. Appl. Pyrolysis* **2025**, *186* paper 106915; <https://doi.org/10.1016/j.jaap.2024.106915>.
- [42] Zhao, S.; Han, Z.; Li, M.; Liu, H.; Mensah, R.A. Das, O.; Jiang, L. Insights into Thermochemistry, Kinetics, and Pyrolysis Behavior of Green Gas Generator 5-Aminotetrazole by Experiment and Theoretical Methods. *Case Stud. Therm. Eng.* **2023**, *49* paper 103217; <https://doi.org/10.1016/j.csite.2023.103217>.

Authorship contribution statement

Jinyu Peng: conception, foundations, performing the experimental part
Bobo Zhang: foundations, methods
Xiang Liu: performing the experimental part, performing the statistical analysis
Liangyou Zhao: methods, performing the statistical analysis
Chongwei An: conception, foundations
Taixin Liang: foundations, performing the experimental part

Submitted: July 21, 2025

Revised: December 19, 2025

First published online: December 31, 2025